

OBSERVATIONS OF THE 599 Hz ACCRETING X-RAY PULSAR IGR J00291+5934 DURING THE 2004 OUTBURST AND IN QUIESCEENCE

M. A. P. TORRES¹, P. G. JONKER^{1,2,3}, D. STEEGHS¹, G. H. A. ROELOFS⁴, J. S. BLOOM⁵, J. CASARES⁶, E. E. FALCO¹, M. R. GARCIA¹, T. R. MARSH⁷, M. MENDEZ^{2,3,8}, J. M. MILLER^{9,1}, G. NELEMANS⁴, P. RODRÍGUEZ-GIL⁶
To appear in the Astrophysical Journal

ABSTRACT

We report on optical and near-infrared observations obtained during and after the 2004 December discovery outburst of the X-ray transient and accretion-powered millisecond pulsar IGR J00291+5934. Our observations monitored the evolution of the brightness and the spectral properties of IGR J00291+5934 during the outburst decay towards quiescence. We also present optical, near-infrared and *Chandra* observations obtained during true quiescence. Photometry of the field during outburst reveals an optical and near-infrared counterpart that brightened from $R \sim 23$ to $R \sim 17$ and from $K = 19$ to $K \sim 16$. Spectral analysis of the *RIJHK* broadband photometry shows excess in the near-infrared bands that may be due to synchrotron emission. The $H\alpha$ emission line profile suggests the orbital inclination is $\sim 22^\circ - 32^\circ$. The preferred range for the reddening towards the source is $0.7 \leq E(B-V) \leq 0.9$, which is equivalent to $4.06 \times 10^{21} \text{ cm}^{-2} \leq N_H \leq 5.22 \times 10^{21} \text{ cm}^{-2}$. The *Chandra* observations of the pulsar in its quiescent state gave an unabsorbed 0.5-10 keV flux for the best-fitting power-law model to the source spectrum of $(7.0 \pm 0.9) \times 10^{-14} \text{ ergs cm}^{-2} \text{ s}^{-1}$ (adopting a hydrogen column of $4.6 \times 10^{21} \text{ cm}^{-2}$). The fit resulted in a power-law photon index of $2.4^{+0.5}_{-0.4}$. The $(R-K)_0$ color observed during quiescence supports an irradiated donor star and accretion disk. We estimate a distance of 2 to 4 kpc towards IGR J00291+5934 by using the outburst X-ray light curve and the estimated critical X-ray luminosity necessary to keep the outer parts of the accretion disk ionized. Using the quiescent X-ray luminosity and the spin period, we constrain the magnetic field of the neutron star to be $< 3 \times 10^8$ Gauss.

Subject headings: accretion, accretion disks — binaries: close — stars: individual: IGR J00291+5934 — X-rays: stars

1. INTRODUCTION

Most known pulsars are isolated neutron stars characterized by pulse (spin) periods of about 0.5 s that increase at a rate of $\dot{P} = dP/dt \sim 10^{-15} \text{ s/s}$ as the rotational kinetic energy is carried away by magnetic dipole radiation (see e.g. Lorimer 2005 and references therein). This implies young neutron stars with characteristic ages of $\tau = P/2\dot{P} \sim 10^7$ years and a magnetic field strength of $B \propto (P\dot{P})^{1/2} \sim 10^{12}$ Gauss. However, a small fraction of this pulsar population has millisecond periods with rotation periods ranging from 1.5 to 30 ms and $\dot{P} \sim 10^{-19} \text{ s/s}$. They are thought to be old neutron stars ($\tau \sim 10^9$ years) with magnetic fields of $B \sim 10^{8-9}$ Gauss. Binary evolution theory predicts that millisecond pulsars are spun-up during mass transfer from the companion star onto the neutron star during the low-mass X-ray binary phase (see e.g. Alpar et al. 1982; Bhattacharya & van den Heuven 1991). This prediction agrees with the wealth of millisecond pulsars found in binary systems ($\sim 80\%$ of the current sample compared to $\lesssim 1\%$ of the young pulsars). Additionally, seven low-mass X-ray

binaries have been found (to date) to harbor an accretion-driven millisecond X-ray pulsar (see e.g. Wijnands 2005a). All seven were discovered as X-ray transients when they underwent an outburst caused by an episode of intense mass transfer onto the neutron star via an accretion disk.

The accretion-driven millisecond X-ray pulsar IGR J00291+5934 was first detected in outburst on 2004 December 2 during Galactic plane scans with *INTEGRAL* (Eckert et al. 2004). Reanalysis of the *Rossi X-Ray Timing Explorer (RXTE) All-sky Monitor (ASM)* data archive showed that the source was likely active during 1998 November and 2001 September, leading to a tentative recurrence time of approximately 3 years (Remillard 2004). Follow-up observations with the *RXTE Proportional Counter Array (PCA)* revealed that IGR J00291+5934 (hereinafter J00291) has a 147.4 min binary orbit and harbors a neutron star spinning at 599 Hz (1.7 ms). To date this is the fastest neutron star spin observed for an accreting powered X-ray pulsar (Markwardt et al. 2004a,b).

Outburst spectra obtained by *INTEGRAL* and *RXTE* are consistent with an absorbed power-law, yielding a pho-

¹ Harvard-Smithsonian Center for Astrophysics, 60 Garden St, Cambridge, MA 02138

² SRON, Netherlands Institute for Space Research, Sorbonnelaan 2, 3584 CA, Utrecht, the Netherlands

³ Astronomical Institute, Utrecht University, P.O.Box 80000, 3508 TA, Utrecht, the Netherlands

⁴ Department of Astrophysics, Radboud University, Toernooiveld 1, 6525 ED Nijmegen, the Netherlands

⁵ Astronomy Department, University of California, Berkeley, CA 94720

⁶ Instituto de Astrofísica de Canarias, 38200 La Laguna, Tenerife, Spain

⁷ Department of Physics, University of Warwick, Coventry CV4 7AL

⁸ Astronomical Institute, University of Amsterdam, Kruislaan 403, 1098 SJ Amsterdam, The Netherlands

⁹ University of Michigan, Department of Astronomy, 500 Church Street, Dennison 814, Ann Arbor, MI 48105, USA

ton index of $\alpha \sim 1.7 - 1.8$ and a hydrogen column of $\geq 2 \times 10^{21} \text{ cm}^{-2}$ (Shaw et al. 2005; Galloway et al. 2005). The *INTEGRAL* spectrum was also well fitted by a thermal Comptonization model with electron temperature of 50 keV and Thomson optical depth ~ 1 (Falanga et al. 2005; Shaw et al. 2005). In addition, the *RXTE PCA* data could be fitted with a two component model: an absorbed power-law and a thermal component with $kT \sim 1$ keV (Paizis et al. 2005), with the thermal component being interpreted as emission originating on a hot spot on the neutron star surface. Whereas the power-law photon index showed no evolution during the outburst decline ($\alpha \sim 1.7$), the thermal component decreased to the point that it could not be constrained with the data acquired 10 days after the outburst onset. A simultaneous *RXTE PCA/Chandra* observation acquired on 2004 December 14 revealed a spectrum in accordance with a 0.4 keV thermal component (associated with emission from the accretion disk) and a power-law component with a similar index as above (Paizis et al. 2005). The *PCA* data also showed that J00291 had a rather uncommon behavior compared to other neutron star low-mass X-ray binaries during outburst: the power spectra showed broad-band flat-top noise with very low break frequencies (0.01–0.1 Hz) as well as the highest integrated fractional *rms* variability ($\sim 50\%$) found to date in neutron star systems. These properties are more similar to those detected in low-hard states of black-hole systems than neutron star systems (Linares, van der Klis & Wijnands 2006). J00291 was observed during quiescence on three occasions with *Chandra*. The first observation was taken a month after its discovery; the second and third observations were taken 12 and 36 days after the initial *Chandra* observation. The analysis of the X-ray spectrum showed clear evidence of X-ray variability during quiescence (Jonker et al. 2005).

The optical and near-infrared counterparts to J00291 were identified with a $R \sim 17$ and $K \sim 16$ mag variable star (Fox & Kulkarni 2004; Steeghs et al. 2004) coincident with the reported radio counterpart (Pooley 2004, Fender 2004). The first spectrum of the optical counterpart indicated the presence of broad emission lines of HeII and H α (Roelofs et al. 2004; see also Filippenko et al. 2004). A binary system with inclination $\lesssim 85$ degrees was supported by the lack of eclipses or dips in the X-ray light curve (Galloway et al. 2005). The donor star in J00291 is likely a hot (irradiated) brown dwarf and not a fully degenerate star given the orbital parameters of the system (Galloway et al. 2005, Falanga et al. 2005) and the presence of hydrogen emission lines in the optical spectrum (Roelofs et al. 2004).

The organization of the paper is as follows: we begin by describing in detail the data acquisition and reduction steps (Section 2). The whole outburst light curve from the monitoring campaign together with photometric observations during quiescence is presented in Section 3. In Section 4 we obtain constraints on the photometric variability of J00291 during outburst and quiescence and in Section 5 we derive a refined astrometric position for the source. The optical spectrum in outburst is analyzed in Section 6. In Section 7 we constrain the reddening towards J00291 and in Section 8 we obtain the optical to near-infrared

spectral energy distribution during outburst. Section 9 presents a detailed analysis of a new *Chandra* observation of J00291 in quiescence. The results are discussed in section 10 where we examine such key questions such as the orbital parameters and distance towards J00291. Our conclusions are summarized in Section 11.

2. OBSERVATIONS AND DATA REDUCTION

2.1. Optical Photometry

Optical photometry of J00291 was obtained with the following telescopes:

The 1.2 m telescope at the Fred Lawrence Whipple Observatory (FLWO) in Arizona. The Minicam mosaic camera was in place and J00291 was imaged with the FLWO Harris *R*-band filter, which closely approximates the Johnson-Cousins *R* broad-band filter. The 0.82 m IAC80 telescope at the Observatorio del Teide on Tenerife using the *R*-band Johnson filter and the Thomson 1024 \times 1024 pixel CCD camera. The 4.2 m Willian Herschel Telescope (WHT) at the Observatorio del Roque de los Muchachos on La Palma using the Aux Port imager which carries a 1024 \times 1024 TEK CCD. The source was observed with the Harris *R* and *I*-band filters with filter transmissions similar to that of Cousins filters. The 2.5 m Isaac Newton Telescope (INT) at La Palma using the Wide Field Camera (WFC), the four thinned EEV 2k \times 4k CCDs and the Harris *R*-band filter. The 3.5 m Telescopio Nazionale Galileo (TNG) at La Palma. Cousins *R* and *I*-band filters were used to acquire images with the DoLoReS instrument equipped with a 2048 \times 2048 Loral CCD. Data were also obtained with the Sloan *r* filter and the MegaCam CCD mosaic camera (McLeod et al. 2000) mounted on the MMT 6.5 m telescope at Mt. Hopkins. Time-resolved photometry of J00291 in quiescence was acquired in the (Harris) *R*-band with the 4.2 m WHT using the Prime Focus Imaging Camera (PFIP) which carries two 2148 \times 4128 EEV CCDs.

Integration times ranged from 100 s to 10 min depending on telescope size, atmospheric conditions and target brightness (see Table 1). The images were corrected for bias and flat-fielded in the standard way using IRAF¹⁰. We performed PSF-fitting photometry (Stetson 1987) on J00291 and several nearby comparison stars. We also performed a photometric calibration of a set of stars in the field of view of J00291 using several standard stars from Landolt plates (Landolt 1992) that were observed with the WHT, the 2.0m Liverpool telescope on La Palma and the FLWO 1.2 m telescope. The magnitudes for J00291 were obtained with differential photometry relative to these local comparison stars.

2.2. Optical Spectroscopy

Ten red and ten blue spectra were acquired on the night of 2004 December 5 using the ISIS double-arm spectrograph attached to the WHT telescope. J00291 was observed using a 1.5 arcsec wide entrance slit with the CCDs on each spectrograph arm binned by two in the spatial direction. The blue arm was used with the R600B grating and the 4096 \times 2048 EEV12 CCD array to yield an useful wavelength coverage of $\lambda\lambda 3500 - 5200$ with a dispersion

¹⁰ IRAF is distributed by the National Optical Astronomy Observatories.

of $0.86 \text{ \AA pix}^{-1}$. The red arm was used with the R600R grating and the 2047×4611 MARCONI2 CCD. The useful wavelength range covered the $\lambda\lambda 5400 - 7100$ interval with a dispersion of $0.88 \text{ \AA pix}^{-1}$. The spectral resolution was about ~ 5.5 pixels FWHM for both arms.

The raw CCD frames were bias and flat-field corrected with standard IRAF routines. The spectra were extracted from each frame with the IRAF KPNOSLIT package. The pixel-to-wavelength calibration was derived from a cubic spline fit (blue spectrum) and a fifth order Legendre polynomial fit (red spectrum) to Copper-Argon and Copper-Neon arc lamp spectra taken at each CCD. The root-mean square (*rms*) deviation of the fit was $< 0.1 \text{ \AA}$ and $< 0.06 \text{ \AA}$ for the data acquired with the blue and red arms respectively. No absolute flux calibration was attempted as the weather conditions were poor. The individual spectra were re-binned into a uniform velocity scale of $60.23 \text{ km s}^{-1} \text{ pix}^{-1}$ (blue) and $41.92 \text{ km s}^{-1} \text{ pix}^{-1}$ (red) to be rectified subsequently by fitting a spline function to the continuum after masking the emission lines.

2.3. Near-infrared photometry

Infrared photometry during the X-ray outburst was obtained from 2004 December 8 to 11 with the 1.3 m Peters Automated Infrared Imaging Telescope (PAIRITEL) at FLWO (Bloom et al. 2006). The camera on PAIRITEL consists of three 256×256 NICMOS3 arrays which image simultaneously a $8.5' \times 8.5'$ field of view in the *J*, *H* and *K_s* photometric bands. The observations consisted of a large number of dithered 7.8 s exposures on source. The dithered exposures were first bias and flat-field corrected to be mosaiced together for each individual visit (see e.g. Blake et al. 2005). Total integration times per visit ranged between 3 to 15 minutes. For each visit, instrumental magnitudes were extracted and consequently calibrated relative to the same nearby 2MASS sources for all exposures. Photometric error estimates on the infrared magnitudes are based on a combination of Poisson statistics and the error contribution of the comparison stars used for each observation.

J00291 was observed on two nights with the 3.8m United Kingdom Infrared Telescope (UKIRT) on Mauna Kea. On December 28 the telescope was equipped with the UKIRT 1.5 micron Imager Spectrometer (UIST; Ramsay Howat et al. 2004). *J*, *H* and *K*-band images were obtained on the 1024×1024 InSb array. Observations consisting of a single 9 point jitter pattern with a 30s exposure at each offset position were performed using the K98 and J98 broad-band filters, giving a total of 4.5 min on source. The same pattern was used with exposures of 60s when using the J98 broad-band filter, yielding 9 min on source. The J98, H98 and K98 filters are the Mauna Kea Observatory NIR Photometric System filters (see Simons & Tokunaga 2002 and Tokunaga et al. 2002 for more details). *K*-band observations were made on 2005 January 24 using the UKIRT Fast-Track Imager (UFTI; Roche et al. 2003) equipped with a 1024×1024 HgCdTe array. The observations were obtained by jittering the image on 9 different positions. Exposures were 30s at each position and the jitter pattern was repeated six times yielding 27 minutes of total on-source observing time. The standard star FS103 from

the set of UKIRT faint standards was observed for photometric calibration. During both nights a dark frame was obtained in each filter at the start of each set of observations. The data were reduced through the automated ORAC-DR pipeline¹¹ (Allan et al. 2002): the individual frames from each filter were bad-pixel masked, dark subtracted, flat-fielded (a flat-field was made using the target frames) and combined to form mosaics. Absolute calibration of the *K*-band mosaic obtained with UFTI was performed with the standard star using a median extinction value of $0.088 \text{ mag airmass}^{-1}$ at the Mauna Kea summit. The resulting absolute magnitudes for the 2MASS stars in the field differed by $\sim 0.05 \pm 0.03$ mag. The small discrepancy is consistent with the expected 2% differences between magnitudes obtained by calibrating with 2MASS and UFTI standard stars (Hodking, Irwin & Hewett 2006; Nikolaev et al. 2000). J00291 was not detected in any of the UIST mosaic frames. These frames were calibrated using 2MASS stars in the field and 3σ upper limits to the near-infrared magnitudes of the source were derived from aperture photometry made to the field stars.

Details of all the observations are summarized in Table 1.

2.4. X-ray data: Observations and reduction

We observed J00291 with the backside-illuminated ACIS-S3 CCD on board the *Chandra* satellite. The observation (ID 6570) started on 2005 November 24 09:49:44 UT. The total on-source time was 24671.5 s. We limited the read-out area of the S3-chip to 1/8th of its original size yielding a smaller exposure time per CCD frame in order to avoid pile-up. The data were reprocessed in a standard way using the ciao 3.3.0 software. We searched the data for periods of enhanced background radiation, but none were found. Hence, all the data were used in our analysis. We extracted the spectrum of J00291 from a circular region with a 3 pixels radius centred on the best-fit source position as provided by *wavdetect*, whereas the background spectrum was extracted using an annulus centred on the source position with inner and outer radius of 10 and 30 pixels, respectively. We detect a total of 143 counts in the source region and 296 in background region. This yields $0.3\text{--}10 \text{ keV}$ background subtracted source count rates of 5.8×10^{-3} counts per second. This rate is so low that pile-up is negligible. The expected background count rate in the source region was 1%.

3. THE OUTBURST LIGHT CURVE

Fig. 1 presents the overall optical/infrared light curve. Each data point represents the mean magnitude per night at each respective band-pass. The discovery optical magnitude ($R \sim 17.4$; Fox & Kulkarni 2004) and the *R*-band photometry reported in Biknaev et al. (2004) have also been included. Note that the follow-up of J00291 could not be continuous as it was hampered by poor weather conditions during the winter season in the Northern Hemisphere.

Our first images were taken on 2004 December 8, and showed the source at $R = 18.33 \pm 0.07$ mag, $I = 17.58 \pm 0.06$ mag, $J = 17.1 \pm 0.1$, $H = 16.7 \pm 0.2$ and $K = 15.9 \pm 0.1$. We fitted an exponential to our first eight

¹¹ <http://www.oracdr.org/>

R-band data points, which describes well the decline in brightness (the *rms* from the fit was 0.11 mag). From the fit we infer a decay rate of 5.2 ± 0.4 d mag $^{-1}$ and thereby an e-folding time of 5.7 ± 0.4 d in flux. Assuming the transient started to decay with the same trend after the outburst peak, the extrapolation of the exponential fit to the time of the discovery by *INTEGRAL* (Eckert et al. 2004, Shaw et al. 2005) yields a peak optical brightness of $R = 17.03 \pm 0.08$ mag. Our JHK_s -band coverage is not sufficient to determine the flux decay rate at near-infrared wavelengths.

In Fig. 2 we plot the *R*-band magnitudes during the initial decay together with the *RXTE PCA* outburst light curve. A first account of the *PCA* light curve is given by Galloway et al. (2005) and Paizis et al. (2005). We digitized their data and plotted them on a logarithmic scale in Fig. 2. This figure shows that the X-ray light curve decays exponentially with an initial e-folding time of 8.5 ± 0.3 d. An exponential decay is expected to happen in short-orbital period binaries such as J00291 because the X-ray irradiation is high enough to ionize the entire accretion disk (King & Ritter 1998; see also discussion). The decay becomes faster after 2004 December 10.2 when the e-folding time becomes 2.6 ± 0.1 d. *INTEGRAL/ISGRI* observations (10-100 keV) also show a change in the rate of decline in the light curve close to 2004 December 10, when the initial 6.6 d e-folding time increases to 2.2 d (Falanga et al. 2005). The optical light curve does not show such a change until 2004 December 15, when there is indication of a steeper decline in the optical brightness. The optical data are consistent with a decay with rate 2.2 ± 0.5 d mag $^{-1}$ (e-folding time of 2.4 ± 0.5 d).

On 2004 December 19, J00291 was found to be at $R = 20.90 \pm 0.06$ mag and it is difficult to assess the light curve morphology due to the lack of coverage after that date. It is possible that the brightness decline slowed down or/and the source underwent mini-outbursts/re-flares in the optical before it reached quiescence. In this regard, the magnitudes reported by Bikmaev et al. (2005; open triangles in Fig. 1) together with our data seem to be consistent with what could have been an optical mini-outburst with amplitude ~ 0.4 mag starting about 2005 January 7 and lasting for about a week. At that time J00291 had definitely ceased its X-ray activity and settled down into quiescence at X-ray wavelengths (Jonker et al. 2005). The unreddened $R - I$ colour during the outburst decline was 0.75 ± 0.09 mag (2004 December 8), 1.1 ± 0.2 mag (2004 December 30) and 0.7 ± 0.3 mag (2005 January 7). We cannot draw any conclusion about the evolution of the color index given the large error bars, which were calculated by adding quadratically the uncertainties on the *R* and *I*-band photometry.

By the end of the possible optical mini-outburst and our outburst follow-up (2005 January 14), the optical magnitude had declined to $r = 22.7 \pm 0.1$. Ten days later, J00291 was imaged with UKIRT to derive a $K = 19.0 \pm 0.1$ magnitude for its near-infrared counterpart in quiescence. Finally, we observed J00291 with the WHT on 2005 October 25/26 to measure a mean magnitude of $R = 23.1 \pm 0.1$ for the optical counterpart in quiescence. This yields a total amplitude for the optical outburst of $\Delta R > 4.8$ mag ($\Delta R = 6.1$ mag from the above extrapolation) and

$$\Delta K > 3.1 \text{ mag.}$$

4. PHOTOMETRIC VARIABILITY

Time-resolved photometry of J00291 over the course of the outburst decline suggested significant short-term variability of amplitude ~ 0.3 mag (Bikmaev et al. 2005; Reynolds et al. 2005), but gave no indication of the orbital period. Our photometric data sets were also searched for short-term photometric variability when more than four data points per night were available. Quantifying the variability of J00291 requires care, since some of our data were acquired under variable weather conditions. We have dealt with this by carrying out photometry of field stars with similar brightness to J00291 or fainter in order to determine the significance of our photometry through the standard deviation on their magnitudes.

Seven images in the JHK_s band-passes were made with PAIRTEL on 2004 December 10. The root-mean-square (*rms*) of the J00291 magnitudes is $0.12 - 0.15$ mag, not different from the comparison stars in the field of view. Any *rms* flux variations of J00291 over the observing interval cannot be much greater than $\sim 15\%$.

We obtained seven *R*-band images during 2004 December 30 with the WHT and six *R*-band images during 2005 January 7 with the TNG. We constrain the *rms* flux variation in J00291 to be $\lesssim 7\%$ and $\lesssim 16\%$ during the small fraction of the orbit covered during the observations (0.15 and 0.087 orbital cycles for the WHT and TNG respectively).

Time-resolved photometry of J00291 in quiescence was acquired on 2005 October 25 with the WHT. We obtained five 300s and twenty 600s *R*-band frames. The *rms* deviation in the photometry over the 1.41 orbital cycles covered by the 600s images (the data with higher s/n ratio) is 0.25 mag, two times larger than the *rms* observed for two fainter comparison stars. The intrinsic *rms* flux variability of J00291 in the *R*-band light curve is constrained to be $\sim 22\%$ by subtracting in quadrature the *rms* flux variation of the comparison stars from the variability observed in J00291. To examine the variability we used both PSF and optimal aperture techniques to determine the magnitudes which gave similar values. We do not see any evidence for orbital modulation in the photometric variability.

5. ASTROMETRY

The position of J00291 was determined using the higher resolution images acquired at different epochs during the outburst decline. These were the images obtained with UKIRT/UFTI (pixel scale of 0.091''/pix), WHT/Aux Port (0.237''/pix), TNG/DoLoReS (0.551''/pix) and MMT/MegaCam (0.160''/pix). The transformation from pixel to sky coordinates was computed using the IRAF tasks *ccmap* and *cctrans* on 6 to 12 bright stars whose PSFs were not corrupted by CCD oversaturation effects. The positions for these internal astrometric reference stars were taken from 2MASS and they have an accuracy of $0.1'' - 0.2''$ (Skrutskie et al. 2004). The *rms* errors of the astrometric fit were $0.05''$ and $0.01''$ (UKIRT), $0.02''$ and $0.07''$ (WHT), $0.05''$ and $0.06''$ (TNG), and $0.06''$ and $0.07''$ (MMT) for right ascension and declination respectively. The error on the position of J00291 provided by the *imcen-*

troid task was always $< 0.03''$. Using the mean of the four measurements we determined a refined position for J00291 of $\alpha(\text{J2000})=00^h29^m03^s.05 \pm 0''.01$ and $\delta(\text{J2000})=+59^\circ34'18''.93 \pm 0''.05$. The errors represent the *rms* of the measurements. The above value is in good agreement with the positions reported for the optical and X-ray counterparts (Fox & Kulkarni 2004; Paizis et al. 2004) and differs from the position for the radio counterpart (Rupen et al. 2004) by 3.2σ in right ascension.

6. THE AVERAGED SPECTRUM

As indicated in Fig. 1, our spectroscopic observations took place on 2004 December 5 during the initial decline of the outburst when the optical brightness was $R=17.72 \pm 0.05$ according to our exponential fit to the optical light curve (Section 3). The data cover 4.5 contiguous hours of spectroscopy representing 1.8 orbital cycles. The individual spectra have a signal-to-noise (s/n) $\lesssim 10$ at 4500 Å and $s/n \sim 10$ at 6300 Å. We produced an average spectrum by assigning optimal weights to the individual spectra to maximize the s/n of the sum. Fig. 3 presents the weighted sum. The spectra show the presence of broad Balmer lines up to likely H δ in emission. The line profile for H α is double-peaked. H β and H δ appear to be double-peaked as well. The high-excitation HeII $\lambda 4686$ emission line is present, but we do not detect the Bowen blend (at $\sim \lambda 4640$). In Table 2 we list the measured line profile parameters: the velocity shift of each line respect to the rest wavelength, the centroid of the line, the FWHM, the peak-to-peak separation, the full width zero intensity (FWZI) and the equivalent width (EW). The values reported are the mean of the measurements obtained by selecting different wavelength intervals to set the underlying continuum and the uncertainties correspond to the standard deviation. Table 2 shows that the emission line profiles are blue-shifted respect to their rest wavelength. This shift more likely reflects the systemic radial velocity (neutron star systems tend to have high systemic velocities; see e.g. White & van Paradijs 1996) and/or the presence of a precessing accretion disk (as observed in short-orbital period X-ray transients in outburst; see e.g. Torres et al. 2002, 2004 and references therein). HeI $\lambda 5875$ in emission seems to be detected. In this regard, HeI $\lambda 6678$ was reported from a single 300s spectrum obtained on 2004 December 12 (Filippenko et al. 2004) when the source brightness was $R=18.93 \pm 0.08$. A visible inspection of this spectrum (see Fig. 1 in Reynolds et al. 2005) shows that HeI $\lambda\lambda 5875, 7065$ emission lines were also present. We measured the EW and radial velocity of the individual H α and HeII $\lambda 4686$ emission line profiles. Neither the EW nor the radial velocities showed clear modulation with the orbital motion.

The main interstellar features detected are the partially resolved atomic Na D doublet at $\lambda\lambda 5889.95, 5895.92$ (total EW of 1.1 ± 0.1 Å) and the CaII $\lambda\lambda 3933.67, 3968.47$ lines (EWs of 0.45 ± 0.02 Å and 0.38 ± 0.04 Å respectively). The spectra show also the presence of diffuse interstellar bands at $\lambda 5780$ (EW=0.4 \pm 0.1 Å), $\lambda 6203$ (EW=0.22 \pm 0.02 Å) and $\lambda 6284$ (EW=1.9 \pm 0.4 Å). The broad 6284 Å band profile is contaminated with telluric O₂. Longward of ~ 6800 Å, the spectra are also contaminated by telluric features.

7. REDDENING TOWARDS J00291

Knowledge of the interstellar extinction is necessary in order to determine the distance to the source and its spectral energy distribution. $E(B-V)$ can be estimated in a number of different ways. From its location in the Galaxy ($l=120.1^\circ$, $b=-3.2^\circ$), the expected color excess is $\lesssim 0.80$ mag according to the average H I column (N_H) obtained by weighting the N_H values within one degree along the line of sight to the source with the inverse of the distance from the source position ($N_H \lesssim 4.66 \times 10^{21} \text{ cm}^{-2}$; Dickey & Lockman 1990). Here we adopt $N_H/E(B-V) = 5.8 \times 10^{21} \text{ cm}^{-2}$ (Bohlin, Savage & Drake 1978). $E(B-V) \lesssim 0.71$ mag using the all-sky reddening maps based on far-infrared emission at 100 μm and 240 μm from dust (Schlegel, Finkbeiner & Davis 1998). Note that both radio and dust maps integrate along the whole line of sight through the Galaxy and that the reddening maps are expected to have reduced accuracy for $|b| < 6^\circ$. Fits to the X-ray spectra acquired with *Chandra* and *RXTE* during the X-ray outburst (Paizis et al. 2004) provided $N_H = 4.3 \pm 0.4 \times 10^{21} \text{ cm}^{-2}$ (High Energy Transmission Grating Spectrometer spectrum - HETGS) and $N_H = 4.3^{+0.7}_{-0.5} \times 10^{21} \text{ cm}^{-2}$ (combined *Chandra* HETGS and *RXTE PCA* spectrum). These values imply a range of $E(B-V) = 0.66 - 0.86$ mag in extinction. Finally, a reddening of $E(B-V) = 0.8 \pm 0.2$ mag can be derived from the calibration between reddening and the EW for the $\lambda 5780$ diffuse interstellar band (Herbig 1993). Note that we use only this interstellar band as it shows a better correlation with reddening than the other diffuse interstellar bands in our spectrum (see Herbig 1975). Based on the above four independent results, we adopt $0.7 \leq E(B-V) \leq 0.9$ ($\equiv 4.06 \times 10^{21} \text{ cm}^{-2} \leq N_H \leq 5.22 \times 10^{21} \text{ cm}^{-2}$) as a likely range of the extinction by giving a lower weight to the result from the $\lambda 5780$ DIB, which is the least precise method for deriving the reddening given the uncertainties in the E(B-V)/EW relationship and the errors in the EW measured for this DIB. The lower limit on $E(B-V)$ yields a dereddened color of $(R-I)_0 = 0.45$ ($R-I = 0.75$; Section 3), indicating a temperature of the order of 5000 K when assuming a thermal origin for the optical flux. This temperature is lower than the > 10000 K temperatures expected in the outer parts of the accretion disk during outburst (see e.g. Hynes 2005) and suggests that $E(B-V)$ is likely larger than 0.7 mag.

8. SPECTROPHOTOMETRIC ENERGY DISTRIBUTION DURING OUTBURST

We acquired simultaneous *JHKs*-band images of J00291 with PAIRITEL during 2004 December 8 to 11. On December 8, 10 and 11 we also obtained *R*-band photometry with the 1.2m at FLWO and observed the source in the *I*-band on December 8. To create spectral energy distributions (SEDs), the optical and infrared magnitudes were dereddened using $A_R(\lambda_c = 0.641\mu\text{m}) = 2.09$ mag, $A_I(\lambda_c = 0.798\mu\text{m}) = 1.49$ mag, $A_J(\lambda_c = 1.235\mu\text{m}) = 0.71$ mag, $A_H(\lambda_c = 1.662\mu\text{m}) = 0.44$ mag and $A_K(\lambda_c = 2.159\mu\text{m}) = 0.29$ mag according to the Cardelli, Clayton & Mathis (1989) extinction law and assuming a reddening $E(B-V)$ of 0.8 mag (as discussed in Section 7). Fluxes were calculated from the magnitudes using the flux calibrations and effective wavelengths specifications for each filter (Bessel 1990; Cohen, Wheaton & Megeath 2003). In

Fig. 4 we plot the infrared to optical SED for three nights. We have also included the near-infrared data acquired on 2004 December 9 for comparison. The errors show the uncertainties in the photometry. The R -band photometry was not simultaneous to the near-infrared observations and to account for this we have overplotted a bar representing the upper limit on the source variability at this bandpass ($\lesssim 0.16$ mag; Section 4). The uncertainty in the reddening correction also contributes to the uncertainty in the SED. The error bars in the bottom of Fig. 4 account for the effect in the flux at each bandpass due to the ± 0.1 mag uncertainty in the reddening.

In X-ray transients in outburst the continuum emission will fall gradually from optical to infrared wavelengths when the thermal spectrum of the X-ray and/or viscously heated accretion disk dominates the flux output at these wavelengths (see e.g. Beall et al. 1984, Vrtilek et al. 1990, Hynes 2005, Russell et al. 2006). Our SEDs show a break in the expected trend at infrared wavelengths where there is significant excess flux in the K -band during the four nights and likely in the H -band on December 11 as well. This supports the presence of another source of near-infrared flux in the spectrum. This source cannot be emission from the donor star as its contribution to the near-infrared flux is $< 8\%$ during outburst. This estimation is based on the K -band magnitudes measured during outburst and in quiescence (Section 3). The near-infrared excess can be explained by invoking optically-thin synchrotron emission, which is expected to contribute to the SED with a component with spectral index $\alpha < 0$ (see Fender 2006 and references therein). This non-thermal component has been claimed to explain the excess of optical/near-infrared flux observed during the outburst of the accreting millisecond X-ray pulsars SAX J1808.4-3658 ($P_{\text{orb}}=2$ hr, Wang et al. 2001; Greenhill, Giles & Coutrou 2006), XTE J0929-314 ($P_{\text{orb}}=43.6$ min, Giles et al. 2005) and XTE J1814-338 ($P_{\text{orb}}=4.3$ hr, Krauss et al. 2005). The detection of mid-infrared optically-thin synchrotron emission from a jet in the neutron star 4U 0614+091 ($P_{\text{orb}} \sim 50$ min; Migliari et al. 2006) adds support to the above claim. For illustration purposes, we show in Fig. 4 a power-law fit ($F_{\nu} \propto \nu^{\alpha}$) to the 2004 December 8 data performed after excluding the flux at the K -band. It is clear that the fit is a poor description of the data: $\chi_{\nu}^2 = 2.4$ and furthermore we cannot exclude the very likely presence of flux excess at H , J -bands and shorter (optical) wavelengths due to the non-thermal (jet) component that will make the SED flatter (redder). The near-infrared unabsorbed flux measured on December 9 (0.30 ± 0.01 mJy at $2.159 \mu\text{m}$, 0.33 ± 0.02 mJy at $1.662 \mu\text{m}$ and 0.43 ± 0.02 mJy at $1.235 \mu\text{m}$) lies above the radio flux of 0.17 ± 0.07 mJy at a frequency of 4.86 GHz measured that day by Rupen et al. (2004; see also Fender et al. 2004). This suggests a spectrum with spectral index ($\alpha \geq 0$), implying a flat or slightly inverted synchrotron optically thick spectrum.

9. X-RAY DATA: ANALYSIS

¹² Note that Jonker et al. (2005) used $N_H = 2.8 \times 10^{21} \text{ cm}^{-2}$ in their work. This value of N_H was derived from preliminary analysis of a 18 ks *Chandra* observation acquired at the end of the X-ray outburst (Nowak et al. 2004) and it has been extensively used in the literature. In the present work, the power-law index and temperature model parameters obtained using $N_H = 2.8 \times 10^{21} \text{ cm}^{-2}$ are consistent within the errors with those obtained using $N_H = 4.6 \times 10^{21} \text{ cm}^{-2}$, whereas the unabsorbed flux is smaller. For comparison, the absorbed and unabsorbed fluxes are $(4.3 \pm 0.9) \times 10^{-14} \text{ ergs cm}^{-2} \text{ s}^{-1}$ and $(6.0 \pm 0.6) \times 10^{-14} \text{ ergs cm}^{-2}$ when N_H was frozen to $2.8 \times 10^{21} \text{ cm}^{-2}$ during the fit.

A month after J00291 went into outburst a 4.7 ks *Chandra* ACIS-S observation detected the source at an unabsorbed flux of $(7.9 \pm 2.5) \times 10^{-14} \text{ ergs cm}^{-2} \text{ s}^{-1}$ (0.5-10 keV). A serendipitous 18 ks observation by *ROSAT* obtained over 1992 July 26 - August 4 also showed J00291 at a similar flux level, confirming its return to quiescence within a month. Additional 9 ks and 12.9 ks *Chandra* observations obtained on 2005 January 13 and 2005 February 6 showed the source at an unabsorbed flux of $(7.3 \pm 2.0) \times 10^{-14} \text{ ergs cm}^{-2} \text{ s}^{-1}$ and $(1.17 \pm 0.22) \times 10^{-13} \text{ ergs cm}^{-2} \text{ s}^{-1}$, revealing that J00291 is variable in quiescence (see Jonker et al. 2005 for more details).

In this section, we analyze an additional 24.6 ks *Chandra* observation acquired on 2005 November 24. We performed a similar spectral analysis to that presented in Jonker et al. (2005) using XSPEC (v11.3; Arnaud 1996). We rebinned the source spectrum such that each bin contains at least 10 counts and used data in the energy range 0.5-10 keV. Due to the low number of source counts per bin, we also checked the spectral fitting results using the Cash statistic (Cash 1979), the results were consistent with those found using chi-squared fitting. For all spectral fits the hydrogen column density towards J00291 was held fixed at $N_H = 4.6 \times 10^{21} \text{ cm}^{-2}$, a likely value of the hydrogen column density as derived in this paper (Section 7).

We began by fitting the spectrum using single component models: a power-law model, a neutron star atmosphere (NSA) model, and a black-body model. For the NSA model we fixed the neutron star magnetic field, its radius and mass at 0 Gauss, 10 km and $1.4 M_{\odot}$, respectively. The temperature and normalization were the only allowed free parameters. The results of these fits are shown in Table 3. As can be seen in Table 3, the single-thermal models did not provide an adequate fit to the data ($\chi_{\nu}^2 > 3.2$) and yield a temperature for J00291 considerably higher than the temperature observed for other neutron star X-ray transients in quiescence. We reject these models on this basis. A single power-law model was statistically acceptable with $\chi_{\text{red}}^2 = 1.2$ for 11 degrees of freedom. In Fig. 5 we have plotted the spectrum showing the power-law fit. The absorbed 0.5-10 keV source flux from the best-fitting power-law model is $(3.8 \pm 1.0) \times 10^{-14} \text{ ergs cm}^{-2} \text{ s}^{-1}$, whereas the unabsorbed flux is $(7.0 \pm 0.9) \times 10^{-14} \text{ ergs cm}^{-2} \text{ s}^{-1}$. We also list in Table 3 the unabsorbed 0.5-10 keV flux derived from other models fit to the data. Note here that the X-ray spectrum of the transient millisecond X-ray pulsars SAX J1808.4-3658 (Campana et al. 2002) and XTE J0929-314 (Wijnands et al. 2005b) are also consistent with an absorbed power-law spectrum. The source flux from the best-fitting power-law model is consistent with the values found using previous *Chandra* and *ROSAT* observations of J00291 during quiescence (Jonker et al. 2005)¹².

Several quiescent neutron star X-ray transients display a soft thermal component plus a hard power-law tail in their spectrum (see e.g. Campana et al. 1998). Our data do not require a two-component model. In order to obtain upper limits on the contribution to the total flux from a

possible thermal component, we fitted the data with this model, consisting of a blackbody or NSA component and the power-law component, both of them modified by the effects of interstellar absorption. We fixed the best fit power law and used 0.2 keV (10⁶ K) for the blackbody (NSA) temperature as in Jonker et al. (2005). In this way we find a 95 per cent upper limit to the fraction of the 0.5-10 keV flux due to a thermal component of < 15% (< 19%).

10. DISCUSSION

10.1. The Outburst Light Curve: Comparison with other Sources

Fig. 2 shows that the X-ray light curve decays exponentially with a break or *knee* where the e-folding time becomes faster. A similar break has clearly been observed in the decay X-ray light curves of three other millisecond pulsars: SAX J1808.4-3658 ($P_{\text{orb}}=2$ hr; Wijnands & van der Klis 1998, Gilfanov et al. 1998, Wijnands 2005a and references therein), XTE J1751-305 ($P_{\text{orb}}=42$ min, Markwardt et al. 2002, Gierliński & Poutanen 2005) and XTE J0929-314 ($P_{\text{orb}}=43.6$ min; Giles et al. 2005, Powell, Haswell & Falanga 2006). In the three systems the break was from an exponential decay to a linear decay (see Powell et al. 2006). A break from a slow to a fast exponential decay has been observed in the light curves of the neutron star X-ray transients Aquila X-1 ($P_{\text{orb}}=18.95$ hr; Maitra & Bailyn 2004) and Centaurus X-4 ($P_{\text{orb}}=15.1$ hr; Evans, Belian & Conner 1970, Kaluzienski et al. 1980; Chen, Shrader & Livio 1997, Shahbaz et al. 1998). The initial exponential decay in the light curves of X-ray transients has been explained assuming that the evolution of the mass in an irradiated disk is described as $\dot{M}_{\text{disk}} = -\dot{M}_c \propto M_{\text{disk}}$, where \dot{M}_c is the central mass accretion rate. Thus $L_x \propto \dot{M}_c = M_{\text{disk}}^0 e^{-t/\tau_e}$ where M_{disk}^0 is the initial mass of the irradiated disk. A faster decay phase (steeper light curve) is expected to occur when the central accretion rate (and thus the X-ray flux) has decreased below the critical X-ray luminosity necessary to keep the outer parts of the disk ionized. Then a cooling front (previously inhibited by X-ray irradiation) will move inwards the disk and switch off the outburst. The rate of decay in the light curve during the propagation of the cooling front has been observed to be either linear or exponential, sometimes showing departures due to one or more secondary maxima that appear during the outburst decline. Details on models for the understanding of the outburst light curves and the outbursts themselves can be found in King & Ritter (1998); Dubus, Hameury & Lasota (2001); Lasota (2001) and Powell et al. (2006).

The ratio of the optical exponential decay time to the X-ray exponential decay time ($\tau_e(\text{opt})/\tau_e(\text{X})$) is expected to be ~ 2 for X-ray transients when the optical flux is dominated by X-ray reprocessing on the disk (King & Ritter 1998). Observational evidence supporting this prediction is that $\langle \tau_e(\text{opt})/\tau_e(\text{X}) \rangle \sim 1.9$ in X-ray novae (Chen et al. 1997). This ratio is $\tau_e(R)/\tau_e(2.5 - 25 \text{ keV}) = 0.67 \pm 0.05$ before the *knee* in the X-ray light curve of J00291. Apart from J00291, SAX J1808.4-3658 is the only millisecond pulsar for which well-sampled optical and X-ray light

curves are available (1998 outburst). For this system we derive¹³ $\tau_e(V)/\tau_e(1.5 - 12 \text{ keV}) = 1.5$. The fact that the decay in the optical light curve of J00291 is faster than observed in X-ray irradiated systems suggests that X-ray heating is insufficient to be the dominant source of optical emission and that viscous dissipation in the disk may make a significant contribution to the optical flux. For instance, the optical light curves of dwarf novae in outburst follow the soft X-rays after the outburst peak ($\tau_e(\text{opt})/\tau_e(\text{X-ray}) \sim 1$) to decline slower than the X-rays a few days later (Jones & Watson 1992, Mauche, Mattei & Bateson 2001, Wheatley, Mauche & Mattei 2003).

The *knee* in the optical light curve of J00291 is delayed ~ 4.7 d with respect to the *knee* in the X-ray light curve (Fig. 2). A delay of ~ 7 d was observed in SAX J1808.4-3658 (Wang et al. 2001). After the *knee*, the optical and X-ray light curves of J00291 decay faster with a similar e-folding time, $\tau_e(R)/\tau_e(2.5 - 25 \text{ keV}) = 0.8 \pm 0.2$. This was not the case during the 1998 outburst of SAX J1808.4-3658, when the flux at optical wavelengths reached a plateau that lasted one month (Wang et al. 2001). The optical decay in J00291 (2.2 ± 0.5 d mag⁻¹; Section 3) is slower than the 0.93 ± 0.05 d mag⁻¹ rate predicted by the relationship for dwarf novae (non-magnetic CVs) between the rate of the decay and the orbital period (Bailey 1975). This is given by Smak (1999) as $(dV/dt)^{-1} = (0.38 \pm 0.02)P_{\text{orb}}(\text{hr})$. In order to use it we have assumed $dR/dt \sim dV/dt$ during the decline of J00291. It is interesting to note that a few intermediate polars (CVs where the accretion disk is disrupted by the magnetic field of the white dwarf as expected in millisecond pulsars) have shown dwarf-nova like outbursts which decay faster than the Bailey's relationship. Examples of these are DO Dra ($P_{\text{orb}}=3.96$ hr, Šimon 2000) and HT Cam ($P_{\text{orb}}=1.35$ hr, Ishioka 2002). In summary, J00291 seems to show during the late decline a longer decay time compared to dwarf novae as has been observed in other X-ray transients. For instance, the optical flux of the neutron star transient XTE J2123-058 ($P_{\text{orb}}=5.96$ hr) decayed with a rate of 5.00 ± 0.02 d mag⁻¹ in the *V*-band and 11.8 ± 0.3 d mag⁻¹ in the *R*-band at the end of the 2000 outburst (Soria, Wu & Galloway 1999, see also Zurita et al. 2000).

10.2. The nature of the donor star

The lack of eclipses or dips in the outburst X-ray light curve imply an inclination $i \lesssim 85^\circ$. This limit combined with the mass function derived from X-ray data ($2.81311 \times 10^{-5} M_\odot$; Galloway et al. 2005) implies a donor star mass $M_2 \geq 0.04$ (0.05) M_\odot for assumed neutron star mass M_1 of 1.4 (2.0) M_\odot . Assuming a random distribution of inclination angles, using the mass function and applying the requirement that the companion fits within its Roche lobe leads to the conclusion that the donor star must be a $\lesssim 0.16 M_\odot$ low-mass star, most likely a brown dwarf bloated by the pulsar X-ray emission (Galloway et al. 2005).

We can use the peak-to-peak separation in the H α emission profile ($\Delta V^{pp} = 650 \pm 40 \text{ km s}^{-1}$) to estimate the inclination of the system by assuming that the peaks in

¹³ $\tau_e(V) = 7.4$ d and $\tau_e(I) = 7.9$ d. These values were obtained using the photometric data from Table 1 in Wang et al. (2001). Only data until MJD 50932.7 were used. $\tau_e(1.5 - 12 \text{ keV}) = 4.89 \pm 0.06$ d (Powell et al. 2006).

the averaged profile represent emission from gas orbiting in the outer radius of the disk with a Keplerian motion. In such a case $\Delta V^{pp} = 2R_{\text{out}}\Omega_K \sin i = 2(GM_1/R_{\text{out}})^{1/2} \sin i$ with R_{out} being the outer disk radius. We take R_{out} to be between the tidal radius R_T (at which the tidal forces of the donor star cut the disk off) and the radius of the 3:1 Lindblad resonance radius $R_{3:1}$ (at which orbits in the disk resonate with the donor-star orbit, driving the disk elliptical). $R_T \sim 0.9R_L(1)$ where $R_L(1)$ is the volume radius of the Roche lobe of the compact star, $R_{3:1} = 3^{-2/3}(1+q)^{-1/3}a$ where $q = M_2/M_1$ and a is the separation between both stellar components (see e.g. Whitehurst & King (1991)). The orbital parameters measured for J00291 allow us to estimate $R_L(1)$ as a function of the mass for the stellar components and a (Eggleton 1983). Using Kepler's third law together with the constraints on the donor and neutron star mass we obtain $1.04 < a(R_\odot) < 1.19$ and $0.56R_\odot = 3.46 \times 10^{10} \text{ cm} < R_{\text{out}} < 0.71R_\odot = 4.96 \times 10^{10} \text{ cm}$. From ΔV^{pp} and R_{out} we estimate a system inclination of $i = \arcsin(1.145 \times 10^{-3}(R_{\text{out}}(R_\odot)/M_1(M_\odot))^{1/2}\Delta V^{pp}(\text{km/s})) \sim 22^\circ - 32^\circ$. This range of inclinations implies a donor star with mass $M_2 = 0.04 - 0.11$ ($0.09 - 0.13$) M_\odot for a $M_1 = 1.4$ (2.0) M_\odot neutron star when using the mass function of the pulsar derived from X-ray data.

As above an upper limit to the inner radius of the H α -emitting regions during outburst (R_{in}) can be obtained by assuming Keplerian motion for the gas. From the maximum velocity extent of the H α line profile ($FWZI = 2400 \pm 100 \text{ km s}^{-1}$) we derive $R_{\text{in}} \lesssim 4GM_1(\sin i/FWZI)^2 = 9.22 \times 10^9 M_1(M_\odot) \sin^2 i \text{ cm}$. This is $\sim 3000 \sin^2 i$ times the corotation radius ($R_{\text{co}} = (GM_1 P_{\text{spin}}^2/4\pi^2)^{1/3} = 2.11 \times 10^6 M_1^{1/3}(M_\odot) \text{ cm}$, where P_{spin} is the neutron star spin period.

From our photometry during quiescence we find $(R - K) = 4.1 \pm 0.1 \text{ mag}$, which corrected from extinction corresponds to an unabsorbed $(R - K)_0$ color of $2.3 \pm 0.3 \text{ mag}$. We plot in Fig. 6 the theoretical mass- $(R - K)$ color tracks for low-mass stars with solar metallicity and ages of 0.1 to 10 Gyr (Baraffe et al. 1998). The Giagayear tracks intersect the mass vs $(R - K)$ diagram at $0.65M_\odot < M_2 < 0.78M_\odot$. For these masses the inclination derived using the mass function is $i \sim 4^\circ - 5^\circ$ which is highly unlikely given the FWHM and the double-peaked profiles of the emission lines, and the fact that the donor star will be much larger than its Roche lobe (Fig. 6). This discrepancy can be explained if the donor star and accretion disk are irradiated by a relativistic particle wind from the pulsar which resumes activity during quiescence (see e.g. Campana et al. 2004) or by residual accretion onto the neutron star surface and by thermal X-ray emission from the pulsar surface which is heated during outbursts (see e.g. Bildsten & Chakrabarty 2001).

10.3. The distance towards J00291

Different methods have been used to constrain the distance. First, Galloway et al. (2005) estimated a lower limit of $\sim 4 \text{ kpc}$ by assuming that the 2004 outburst fluence is typical for the system and that the mass transfer rate is driven by gravitational radiation. These authors suggested that the distance cannot be much larger based on the fact that thermonuclear bursts were not detected during the

outburst event. Second, Jonker et al. (2005) derived a distance of $2.6 - 3.6 \text{ kpc}$ by assuming that the source quiescent X-ray luminosity of J00291 is similar to that measured for the millisecond pulsars SAX J1808.4-3658 and XTE J0929-314 in quiescence. Using SAX J1808.4-3658 alone (for which $d = 3.4 - 3.6 \text{ kpc}$, Galloway & Cumming 2006) and the unabsorbed flux of J00291 during quiescence measured in Section 8, we roughly estimate the distance towards J00291 to be $2.0 - 3.4 \text{ kpc}$.

The distance to J00291 can be constrained using the critical X-ray luminosity necessary in a neutron-star X-ray transient to heat the disk and produce an exponential decay light curve. We can estimate the distance to J00291 by assuming that the X-ray irradiation was until the knee high enough to ionize the whole disk. Shahbaz et al. (1998) following King & Ritter (1998) derived expressions for the critical X-ray luminosity necessary to keep the disk ionized everywhere. For a neutron star system they found $L_{\text{crit}} = 3.7 \times 10^{36} R_{11}^2 \text{ ergs s}^{-1}$ where R_{11} is the ionized disk radius in units of 10^{11} cm . The disk radius will be between R_{out} and the circularization radius as most of the disk mass will be accreted during the outburst event. The circularization radius is given by $R_{\text{circ}}/a = (1+q)(R_{L1}/a)^4$ (see e.g. Frank et al. 1992) where R_{L1} is the distance between the center of the compact object and the inner Lagrangian point for the donor star. R_{L1} can be approximated in function of q (see e.g. Warner et al. 1995). Using our constraints on a and q we obtain $2.30 \times 10^{10} \text{ cm} < R_{\text{circ}} < 3.68 \times 10^{10} \text{ cm}$. From R_{out} and R_{circ} we estimate $L_{\text{crit}} = 2.0 - 9.1 \times 10^{35} \text{ ergs s}^{-1}$ and from our fit to the X-ray light curve we derive an unabsorbed X-ray flux of $\sim 5 \times 10^{-10} \text{ ergs cm}^{-2} \text{ s}^{-1}$ at the time of the knee. Combining both results we found a distance of 1.8 to 3.8 kpc, in line with previous estimates by Jonker et al. (2005). Taking the apparent R - and K -band magnitudes during quiescence (Section 3) and the reddening at these band passes (Section 8), we derive from the distance module $\log d(\text{pc}) > (5.2 \pm 0.3) - M_R/5$ and $\log d(\text{pc}) > (4.7 \pm 0.1) - M_K/5$. These are lower limits to the distance towards J00291 as both donor star and disk are irradiated by the pulsar. In Fig. 7 we show the predicted mass-absolute magnitude diagram for low-mass stars with ages of 0.1 to 10 Gyr and the mass-distance diagram derived from the distance module.

10.4. Constraints on the neutron star magnetic field

Following Burderi et al. (2002) and Di Salvo & Burderi (2003), we can put constraints on the neutron star magnetic momentum and thereby the magnetic field strength B by comparing the X-ray luminosity measured in quiescence with the expected X-ray luminosity due to residual accretion onto the neutron star or magnetic dipole radiation. The X-ray luminosity originated in these (mutually exclusive) processes depends on both the pulsar spin frequency and B (see Burderi et al. 2002). Thermal emission from the neutron star may also contribute to the quiescent X-ray emission (section 9) and therefore these constraints represent upper limits only. The spin period of the pulsar in J00291 is 1.67 ms (Galloway et al. 2005). The 0.5-10 KeV quiescent X-ray luminosity is $L_x \sim 3.4 \times 10^{31} - 1.3 \times 10^{32} \text{ ergs s}^{-1}$ (range due to our uncertainty in the distance). Considering the above processes

and using the equations derived in Di Salvo & Burderi (2003), the neutron star magnetic field is most likely less than $2 - 4 \times 10^8$ Gauss (a neutron star with mass $1.4 M_{\odot}$ and a radius 10 km was adopted). For comparison, the magnetic field of the neutron stars in the millisecond pulsars SAX J1808.4-3658 ($P_{\text{spin}} \sim 2.5$ ms), XTE J1751-305 ($P_{\text{spin}} \sim 2.3$ ms) and XTE J0929-314 ($P_{\text{spin}} \sim 5.4$ ms) are constrained to be $(1 - 5) \times 10^8$ Gauss, $< 3 \times 10^9$ (d/10 kpc) Gauss and $< (3 - 7) \times 10^8$ (d/8 kpc) Gauss respectively (Di Salvo & Burderi 20003, Wijnands et al. 2005b).

11. CONCLUSIONS

In this paper we have presented multiwavelength observations of the millisecond pulsar IGR J00291+5934. The best source position derived from the optical and near-infrared images is $\alpha(\text{J2000}) = 00^h 29^m 03^s.05 \pm 0^s.01$ and $\delta(\text{J2000}) = +59^{\circ} 34' 18''.93 \pm 0''.05$. From the spectral analysis of our broadband photometry we found strong evidence for excess in the near-infrared bands that may be due to synchrotron emission. We find that the most likely range for the reddening towards J00291 is $0.7 \leq E(B - V) \leq 0.9$ ($\equiv 4.06 \times 10^{21} \text{ cm}^{-2} \leq N_H \leq 5.22 \times 10^{21} \text{ cm}^{-2}$). The X-ray spectrum of the source is well-fitted with a power-law model with photon index $2.4^{+0.5}_{-0.4}$. The unabsorbed quiescent 0.5-10 keV flux is $(7.0 \pm 0.9) \times 10^{-14}$ ergs $\text{cm}^{-2} \text{ s}^{-1}$ for $N_H = 4.6 \times 10^{21} \text{ cm}^{-2}$. At least 81 % of the flux in the 0.5-10 keV range is due to this model. The $(R - K)_0$ color index observed during quiescence supports an irradiated low-mass donor star and accretion disk. We estimate an inclination of $\sim 22^{\circ} - 32^{\circ}$ based on the H α emission line profile and we constrain the distance towards J00291 from 2 to 4 kpc. The magnetic field of the neutron star is most likely $< 2 - 4 \times 10^8$ Gauss.

In contrast with the longer recurrence times for X-ray novae, several millisecond pulsars undergo outbursts in an interval of a few years. This fact opens the opportunity of obtaining a large sample of multiwavelength outburst light curves for these X-ray sources, making possible a future statistical analyses of their light curves as it has been done for the dwarf novae outbursts. The outburst light curves of millisecond pulsars may clarify the role that X-ray irradiation plays in the framework of the thermal instability model both for neutron star and black hole X-ray transients. Finally, the monitoring of an outburst should span a large spectral range to allow us to understand the emission mechanisms in these systems.

We thank Jeff McClintock for comments on the manuscript. DS acknowledges a Smithsonian Astrophysical Observatory Clay Fellowship. This work was supported in part by NASA LTSA grant NAG5-10889 and NASA contract NAS8-39073 to the Chandra X-Ray Center. JSB is partially supported through a Sloan Research Fellowship. The Peters Automated Infrared Imaging Telescope (PAIRITEL) is operated by the Smithsonian Astrophysical Observatory (SAO) and was made possible by a grant from the Harvard University Milton Fund, the camera loan from the University of Virginia, and the continued support of the SAO and UC Berkeley. Partial support for the PAIRITEL project was also supplied by a NASA Swift Cycle 1 & 2 Guest Investigator grants. UKIRT is operated by the Joint Astronomy Center, Hilo, Hawaii, on behalf of the U.K. Particle Physics and Astronomy Research Council. We would like to thank the UKIRT Service Observing Programme for obtaining the data.

REFERENCES

Allan, A., Jenness, T., Economou, F., Currie, M. J., & Bly, M. 2002, Astronomical Data Analysis Software and Systems XI, ASP Conference Proceedings, Vol. 281, eds. D. A. Bohlender, D. Durand, & T. H. Handley (San Francisco:ASP), 311

Alpar, M. A., Cheng, A. F., Ruderman, M. A., Shaham, J. 1982, Nature, 300, 728

Bailey, J. 1975, Brit. astr. Ass., 86, 30

Baraffe, I., Chabrier, G., Allard, F., Hauschildt, P. H. 1998, A&A, 337, 403

Baraffe, I., Chabrier, G., Barman, T. S., Allard, F., Hauschildt, P. H. 2003, A&A, 402, 701

Beall, J. H., Knight, F. K., Smith, H. A., Wood, K. S., Lebofsky, M., Rieke, G. 1984, ApJ, 284, 745

Bessell, M. S. 1990, PASP, 102, 1181

Bhattacharya, D. & Verbunt, F. 1991, PhR, 203, 1

Bikmaev, I. et al. 2004, ATel 395

Bildsten, L. & Chakrabarty D. 2001, ApJ, 557, 292

Blake, C. E. et al. 2005, Nature, 435, 181

Bloom J. S., Starr D. L., Blake C. H., Skrutskie M. F., Falco E. E. 2006, in Astronomical Data Analysis Software and Systems XV, ASP Conference Series, Vol. 351, C. Gabriel, C. Arviset, D. Ponz and E. Solano, eds.

Bohlin, R. C., Savage, B. D. & Drake, J. F. 1978, ApJ, 224, 132

Burderi et al. 2002, ApJ, 574, 930

Campana, S., Colpi M., Mereghetti, S., Stella, L., Tavani, M. 1998, A&ARv, 8, 279

Campana et al. 2002, ApJ, 575, 15

Campana et al. 2004, ApJ, 614, 49

Campana, S., Ferrari, N., Stella, L., Israel, G. L. 2005, A&A, 434, 9

Cardelli, J. A., Clayton, G. C., Mathis, J. S. 1989, ApJ, 345, 245

Cash W. 1979, ApJ, 228, 939

Cohen, M., Wheaton, WM. A., Megeath, S. T. 2003, AJ, 126, 1090

Chabrier, G., Baraffe, I., Allard, F., Hauschildt, P. 2000, ApJ, 542, 464

Chen, W., Shrader, C. R., Livio, M. 1997, ApJ, 491, 312

Di Salvo, T. & Burderi, L. 2003, A&A, 397, 723

Dickey, J. M., & Lockman, F. J. 1990, ARA&A, 28, 215

Dubois, G., Hameury, J.-M., Lasota, J.-P. 2001, A&A, 373, 251

Eckert et al. 2004, ATel 352

Eggleton, P. P. 1983, ApJ, 268, 368

Evans, W. D., Belian, R. D. & Conner, J. P. 1970, ApJ, 159, L57

Falanga et al. 2005, A&A, 444, 15

Fender, R., De Bruyn, G., Pooley, G., Stappers, B. 2004, ATel 361

Fender, R. 2006, in Compact Stellar X-ray Sources, eds. W. H. G. Lewin and M. van der Klis, in press (astro-ph/0303339)

Filippenko, A. V., Foley, R. J. & Callanan, P. J. 2004, ATel 366

Fox, D. B. & Kulkarni, S. R. 2004, ATel 354

Frank, J., King, A. & Raine, D. 1992, Accretion Power in Astrophysics (Cambridge: Cambridge Univ. Press)

Galloway, D. K., Markwardt, C. B., Morgan, E. H., Chakrabarty, D. & Strohmayer, T. E. 2005, ApJ, 622, L45

Galloway, D. K., Cumming, A. 2006, ApJ, 652, 559

Gierliński, M. & Poutanen, J. 2005, MNRAS, 359, 126

Giles, A. B., Greenhill, J. G., Hill, K. M., Sanders, E. 2005, MNRAS, 361, 1180

Gilfanov, M., Revnivtsev, M., Sunyaev, R., Churazov, E. 1998, A&A, 338, L83

Greenhill, J. G., Giles, A. B. Coutures, C. 2006, MNRAS, 370, 1303

Herbig, G. H. 1975, ApJ, 196, 129

Herbig, G. H. 1993, ApJ, 407, 142

Hodkin, S., Irwin, M. & Hewett, P. 2006, CASU WFCAM/VISTA documentation. No VDF-TRE-IOA-00011-00001

Hynes, R. 2005, ApJ, 623.1026

Ishioka, R., Kato T., Uemura, M., Billings G. W., Morikawa K., Torii K., Tanabe K., Oksanen A., Hyvnen H., Itoh H. 2002, PASJ, 54, 5811

Jones, M. H. & Watson, M. G. 1992, MNRAS, 257, 663

Jonker, P. G., Wijnands, R., van der Klis, M. 2004, MNRAS, 349, 94

Jonker, P. G., Campana, S., Steeghs, D., Torres, M. A. P., Galloway, K. K., Markwardt, C. B. & Chakrabarty, D. 2005, MNRAS, 361, 511

Jonker P. G., Galloway D. K., McClintock J. E., Buxton M., Garcia M., Murray S. 2004, MNRAS, 354, 666

Kaluzienski, L. J., Holt, S. S., Swank, J. H. 1980, ApJ, 241, 779

King A., & Ritter, H. 1998, MNRAS, 293, 42

Krauss et al. 2005, ApJ, 627, 910

Landolt, A. U. 1992, AJ, 104, 340

Lasota, J.-P. 2001, NewA Rev, 45, 449

Linares, M., van der Klis, M., Wijnands, R. 2006, submitted to ApJ (astro-ph/0610902)

Lorimer, D. R. 2005, Living Reviews in Relativity, vol. 8, no 7

Maitra, D. & Bailyn, C. 2004, ApJ, 608, 444

Markwardt, C. B., Swank J. H., Strohmayer, T. E., Zand, J. J. M. int., Marshall, F. E. 2002, ApJ, 575, 21

Markwardt, C. B., Swank, J. H. & Strohmayer, T. E. 2004a, ATel 353

Markwardt, C. B., Galloway, D. K., Chakrabarty, D., Morgan, E. H. & Strohmayer, T. E. 2004b, ATel 360

Mauche, C. W., Mattei, J. A., Bateson, F. M. 2001, ASP Conf. Ser. 229, in Evolution of Binary and Multiple Stars, ed. P. Podsiadlowski et al. (San Francisco: ASP), 367

McLeod, B. A., Conroy, M., Gauron, T. M., Geary, J. C., & Ordway, M. P. 2000, Further Developments in Scientific Optical Imaging, 11

Migliari, S., Tomsick, J. A., Maccarone, T. J., Gallo, E., Fender, R. P., Nelemans, G., Russell, D. M. 2006, ApJ, 643, 41

Nikolaev, S., Weinberg, M. D., Skrutskie, M. F., Cutri, R. M., Wheelock, S. L., Gizis, J. E., Howard, E. M. 2000, AJ, 120, 3340

Nowak et al. 2004, ATel 369

Paizis, A., Nowak, M. A., Wilms, J., Courvoisier, T. J-L., Ebisawa, K., Rodriguez, J. & Ubertini, P. 2005, A&A, 444, 357

Pooley, G. 2004, ATel 355

Powell, C. R., Haswell, C. A., Falanga, M. 2006, in press (astro-ph/0610108)

Ramsay Howatt, S. K et al. 2004, in Proc Spie 5492, UV and Gamma-Ray Space Telescope Systems, eds. Hasinger G., Turner M.J., p.1160

Remillard, R. 2004, ATel 357

Reynolds, M. T. et al. 2006, in Populations of High Energy Sources in Galaxies. Proceedings of the 230th Symposium of the IAU, ed. E. J. A. Meurs, G. Fabbiano, Cambridge: Cambridge University Press. 230, 80

Roche, P.F. et al. 2003, Proc Spie 4841, Instrument Design and Performance for Optical/IR Ground-Based Telescopes, eds. M Iye and A.F Moorwood)

Roeofs, G., Jonker, P. G., Steeghs, D., Torres, M. & Nelemans, G. 2004, ATel 356

Rupen, M. P., Dhawan, V., Mioduszewski, A. J. 2004, ATel 364

Russell, D. M., Fender, R. P., Hynes, R. I., Brocksopp, C., Homan, J., Jonker, P. G., Buxton, M. M. 2006, MNRAS, 371, 1334

Schlegel, D. J., Finkbeiner, D. P., Davis, M. 1998, ApJ, 500, 525

Shahbaz, T., Charles, P. A., King, A. R. 1998, MNRAS, 301, 382

Shaw, S. E., Mowlavi, N., Rodriguez, J. et al. 2005, A&A, 432, L13

Simons, D. A. & Tokunaga, A. 2002, PASP, 114, 169

Simon, V. 2000, A&A, 360, 627

Skrutskie, M. F. et al., AJ, 131, 1163

Smak, J. 1999, AcA, 49, 391

Soria, R., Wu, K., Galloway, D. K. 1999, MNRAS, 309, 528

Steeghs, D., Blake, C., Bloom, J. S., Torres, M. A. P., Jonker, P. G., Starr, D. 2004, ATel 363

Stetson, P. B. 1987, PASP, 99, 191

Tokunaga, A. T., Simos, D. A. & Vacca, W. D. 2002, PASP, 114, 180

Torres et al. 2002, ApJ, 569, 423

Torres et al. 2004, ApJ, 612, 1026

Vrtilek, S. D., Raymond, J. C., Garcia, M. R., Verbunt, F., Hasinger, G., Kurster, M. 1990, A&A, 235, 162

Wang et al. 2001, ApJ, 563, L61

Warner, B. 1995 in Cataclysmic Variable Stars, (Cambridge University Press: Cambridge)

Wheatley, P. J., Mauche, C. W., Mattei, J. A. 2003, MNRAS, 345, 49

White, N. E. & van Paradijs, J. 1996, ApJ, 473, 25

Whitehurst, R. & King, A. 1991, MNRAS, 249, 25

Wijnands, R. & van der Klis, M. 1998, ApJ, 507, 63

Wijnands, R., Homan, J., Heinke, C. O., Miller, J. M., Lewin, W. H. G. 2005b, ApJ, 619, 492

Wijnands, R., Homan, J., Miller, J. M., Lewin, W. H. G. 2005, ApJ, 606, 61

Wijnands, R. 2005a, in Pulsars New Research (NY: Nova Science Publishers), in press, astro-ph/0501264

Zurita, C., Casares, J., Shahbaz, T., Charles, P. A., Hynes, R. I., Shugarov, S., Goransky, V., Pavlenko, E. P., Kuznetsova, Y. 2000, MNRAS, 316, 137

Zurita, C. et al. 2002, MNRAS, 334, 999

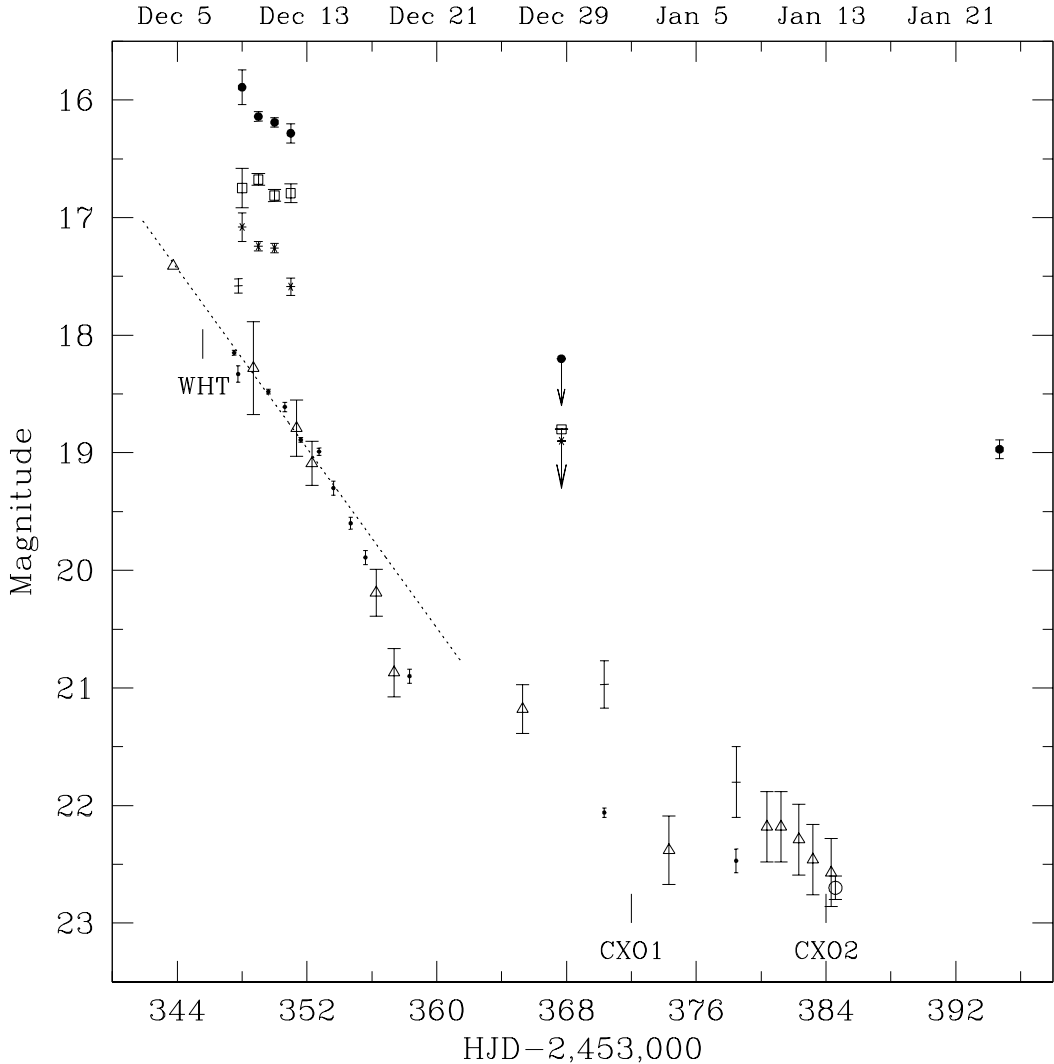


FIG. 1.— Optical and near-infrared light curve of J00291 covering the 2004 December-2005 January outburst. Optical and infrared data points are: R_c and R Johnson (dots), r (open circle), I_c and I Johnson (crosses), J (crosses), H (open squares) and K_s (filled circles). Open triangles mark R band magnitudes reported by Fox & Kulkarni (2004) and Bikmaev et al. (2005). The latter were taken by digitizing the published light curve. Arrows denote upper limits. The dotted curve shows the first exponential fit described in Section 3. For the sake of comparison this curve is plotted from 2004 December 2 09:00:19 UTC (source discovery with *INTEGRAL*) to 2004 December 22 00:00. Times of the WHT spectroscopy during outburst and *Chandra X-ray observatory* (CXO) observations during quiescence (Jonker et al. 2005) are marked as WHT and CXO1, CXO2 respectively. The third CXO observation on MJD 53407.57 is not shown.

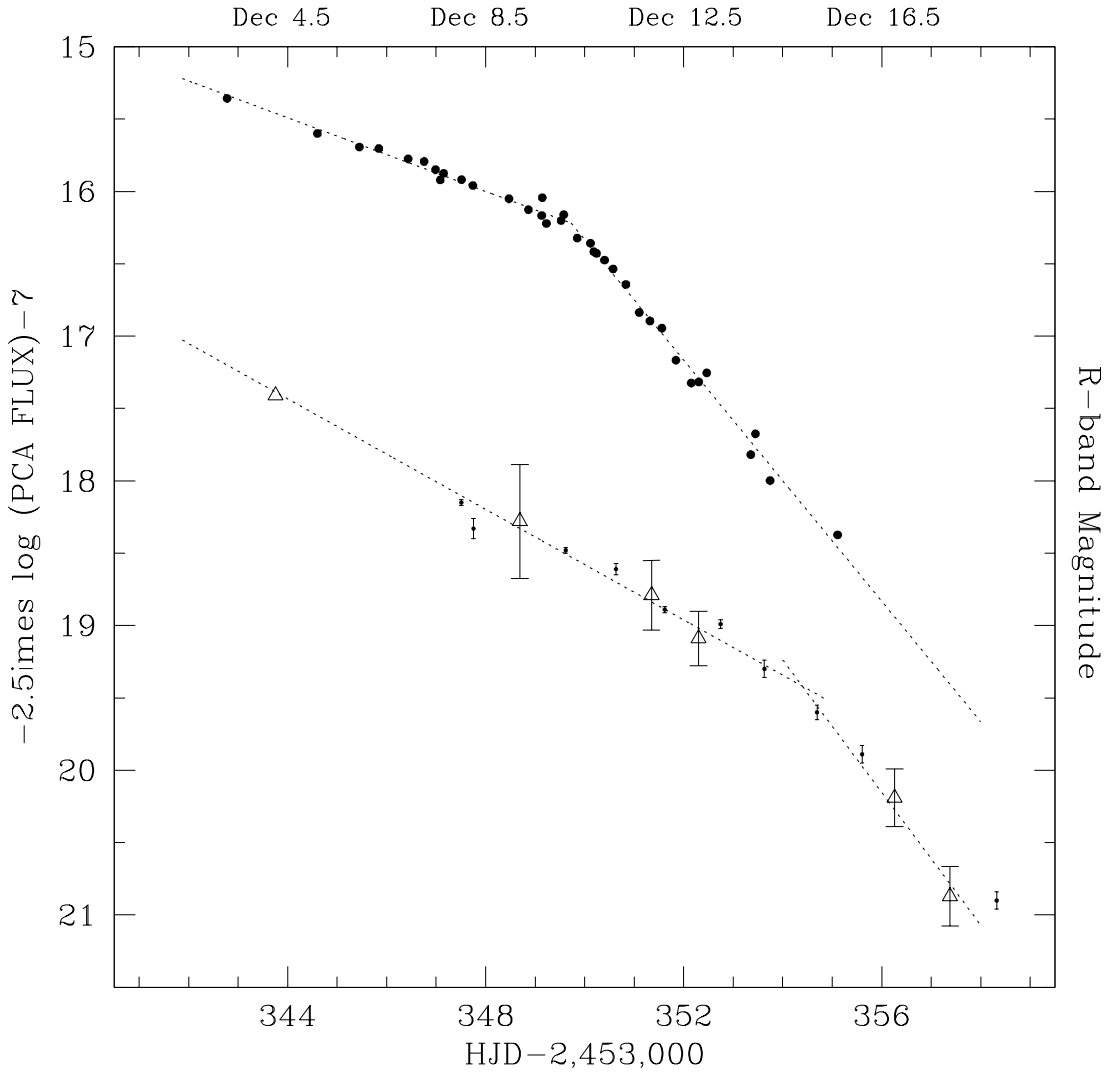


FIG. 2.— *RXTE/PCA* (2.5-25 keV) and *R*-band outburst light curves of J00291 bracketing the 2004 December 2 to 2005 December 19 outburst interval. The dotted curves show the exponential fits to the data. The scale in the Y-axes is the same for the optical and X-ray data. The symbols in the *R*-band (lower) light curve are the same as in Figure 1.

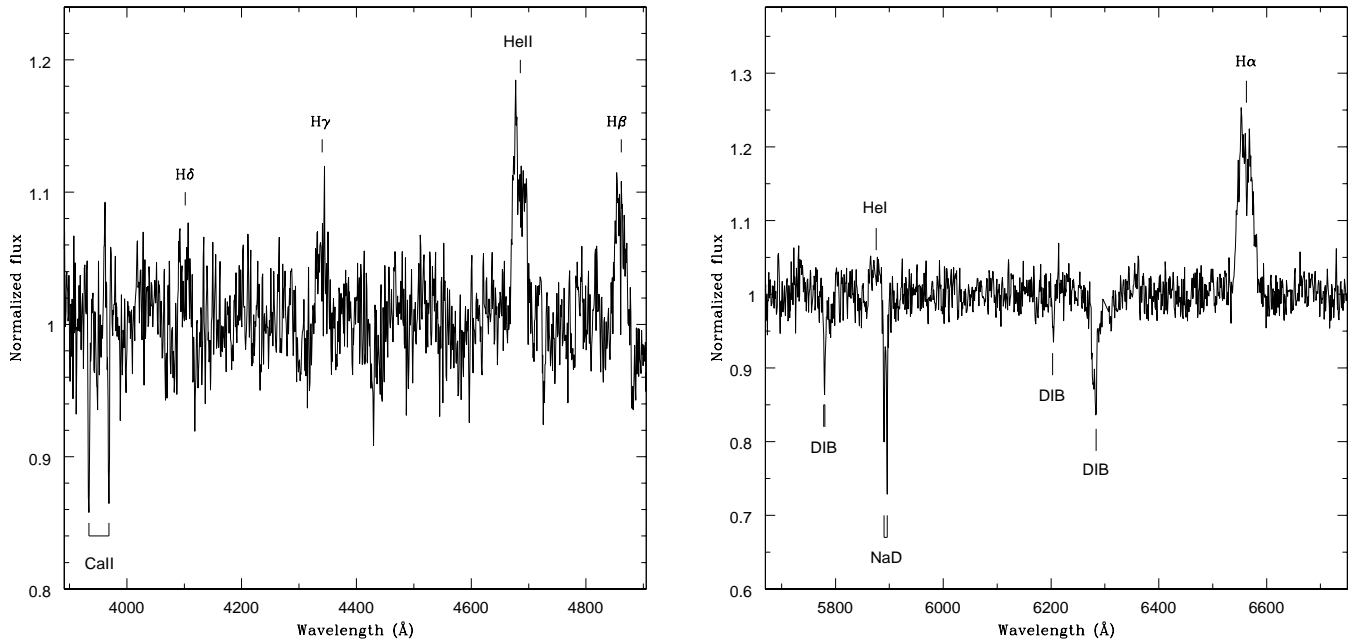


FIG. 3.— The normalized and averaged optical spectrum of J00291. Major disk and interstellar features are identified. DIB denotes the diffuse interstellar bands.

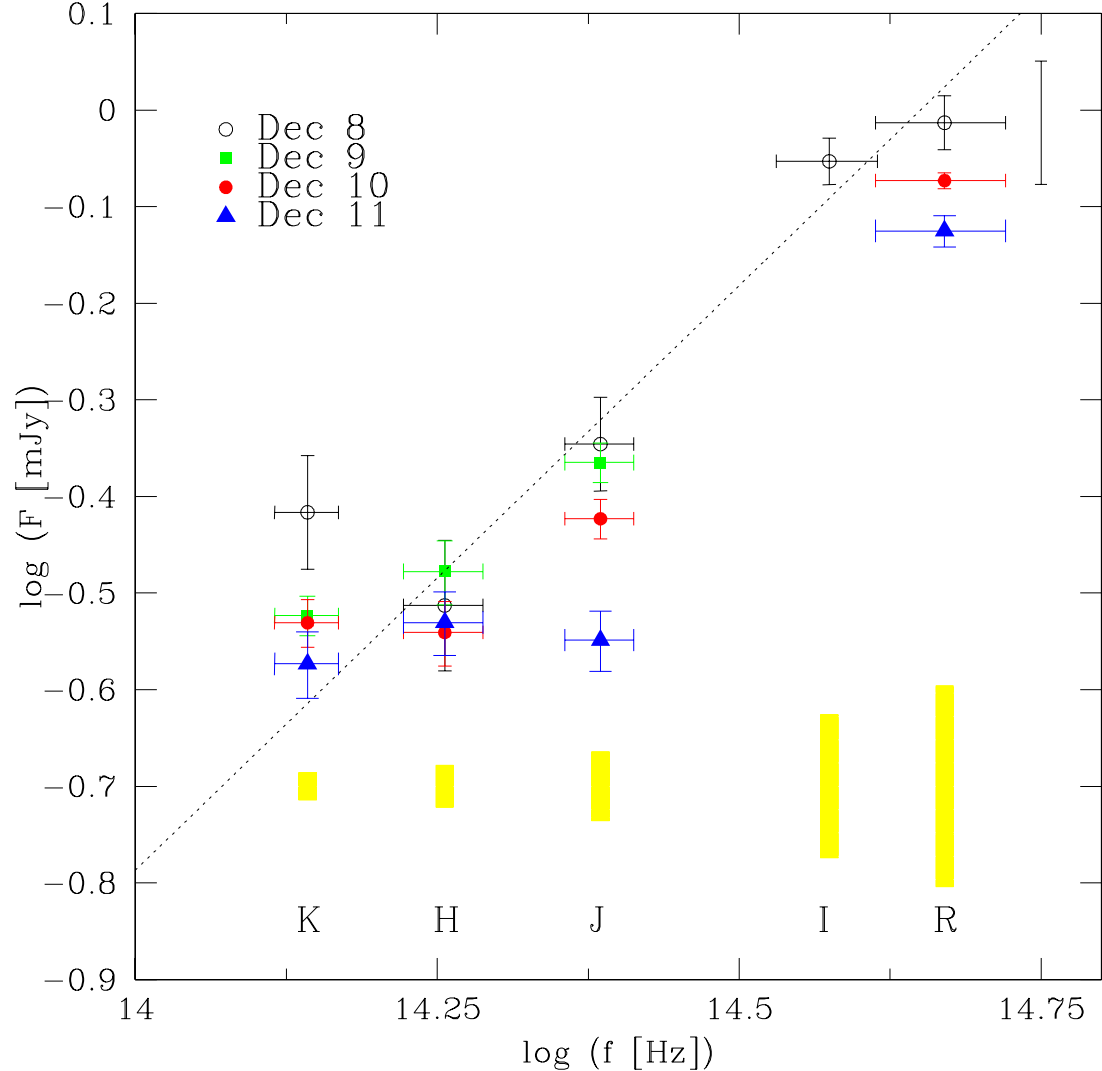


FIG. 4.— Optical/near-infrared spectral energy distribution of J00291 on 2004 December 8, 9, 10 and 11. The fluxes in each band have been dereddened with $E(B-V)=0.8$ mag as described in Section 7. The error bars of the data are the uncertainties in the photometry, whereas the isolated vertical bar represents the upper limit of the observed flux variation at optical wavelengths. Horizontal error bars are the K_s , H , J , I_c and R_c filter bandwidths. Overdrawn as bars are the effects in the flux (at the central wavelength of each bandpass) due to the uncertainty (± 0.1 mag) in the reddening. We also show the power-law fit to the December 8 data after excluding the K -band flux (dotted line). The fit yields $\alpha = 1.2 \pm 0.2$.

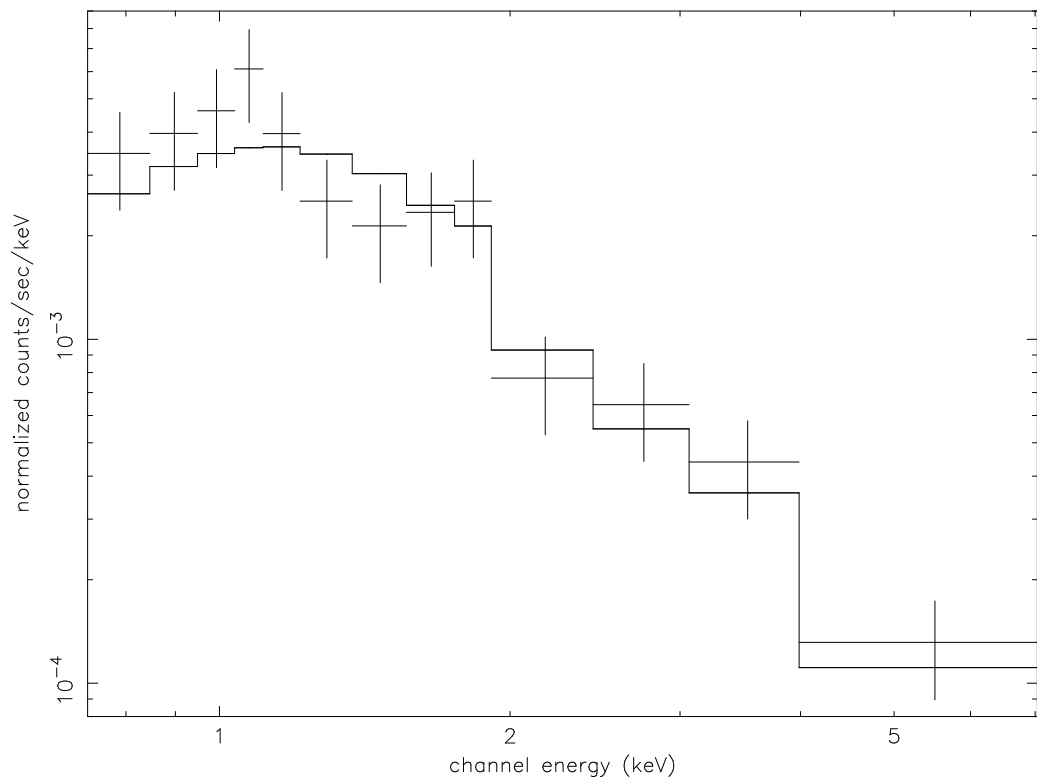


FIG. 5.— X-ray spectrum of J00291 obtained during quiescence. The solid line through the spectrum is the best-fit absorbed power-law model with $N_H = 4.6 \times 10^{21} \text{ cm}^{-2}$.

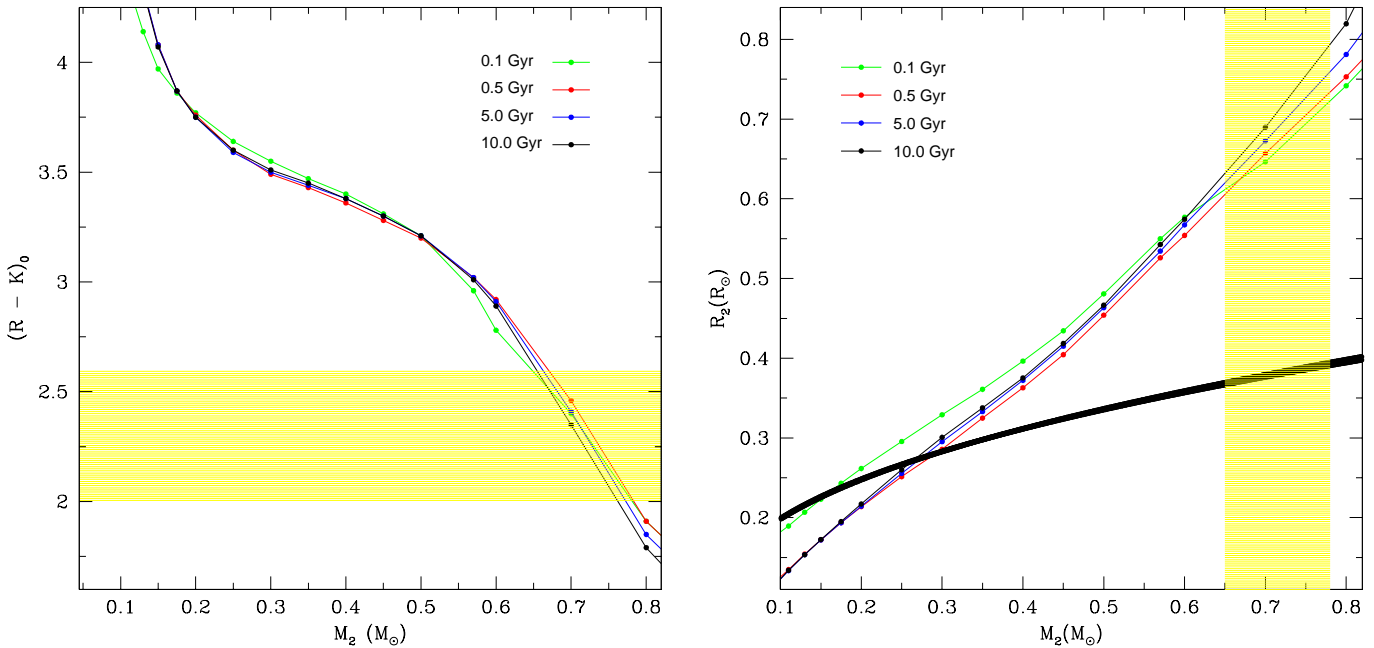


FIG. 6.— Left: Predicted color ($R - K$) as a function of the mass for low-mass stars with ages 0.1, 0.5, 5 and 10 Gyr. Isochrones are taken from Baraffe et al. (1998). The shadowed region delineates our constraint on the ($R - K$) quiescent color of J00291. Right: Predicted radius vs mass diagram for low-mass stars as derived from the isochrones presented in the left panel of the figure. The thick solid line represents the Roche lobe of the donor star when adopting a neutron star mass of $1.4 - 2.0 M_\odot$.

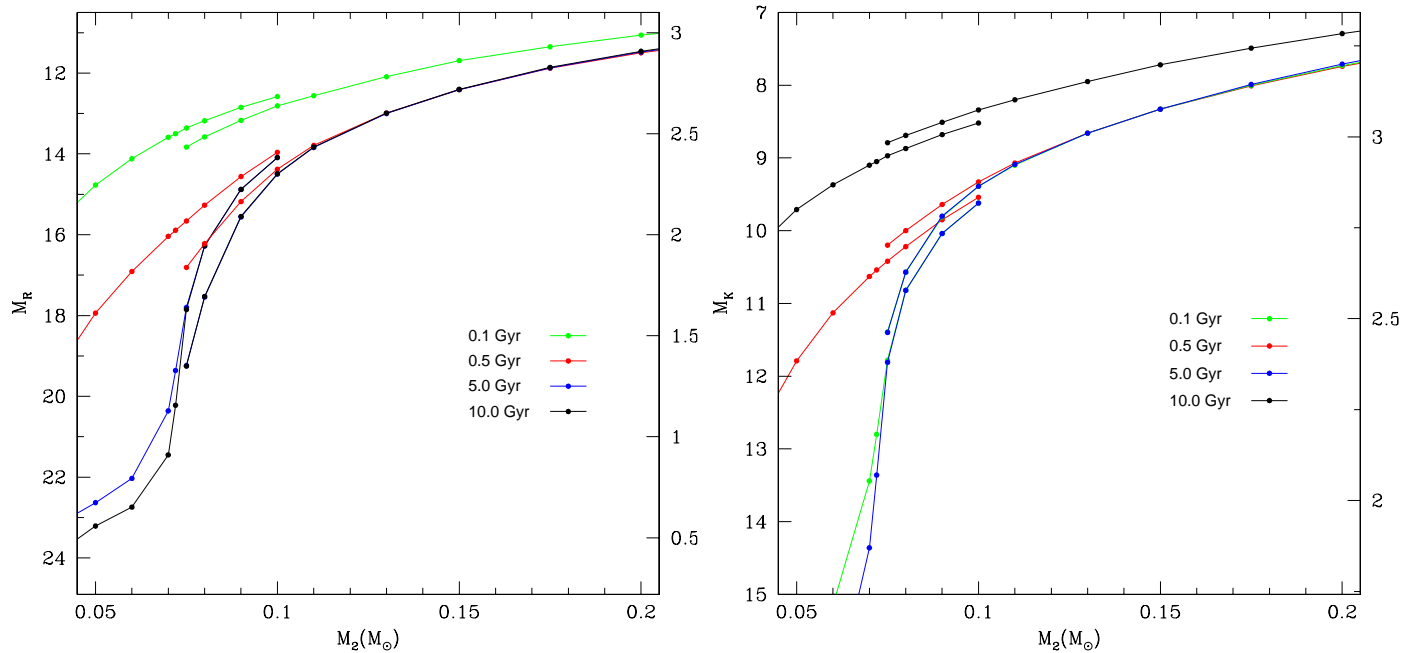


FIG. 7.— Predicted M_R (left) and M_K (right) as a function of the mass. Isochrones are taken from Baraffe et al. (1998) for masses $\geq 0.075 M_\odot$ and Baraffe et al. (2003) for masses $\leq 0.01 M_\odot$. The mismatch between isochrones in the range $0.075 M_\odot$ - $0.01 M_\odot$ reflect model differences. The right-band-side axes are the logarithm of the upper limit to the distance (in pc) towards J00291 given by $5.2 - M_R/5$ and $4.7 - M_K/5$ (see Section 10.3).

TABLE 1
JOURNAL OF OBSERVATIONS

Date (UT)	HJD start-end (+2,453,000.)	Telescope	Bandpass/ Spectral range (Å)	No. Images/Spectra	Exp. time (s)	seeing (arcsec)
OUTBURST						
04 Dec 5	345.39379-345.58101	WHT	3500-5200 5400-7100	10	830-1500	> 1.5
04 Dec 8	347.50266-347.51439	IAC80	R	10	”	”
	347.75290-347.76292	1.2m	R,I	3	300	2.1
	347.71597-347.72639	PAIRITEL	J,H,Ks	2,2	60,60	3.2,3.7
04 , 9	348.56496-348.63947	PAIRITEL	”	1	439	
04 , 10	349.60736-349.62958	1.2m	R	3	188,424,926	2.7
	349.55555-349.69166	PAIRITEL	J,H,Ks	4	300	2.4
04 , 11	350.62887-350.63983	1.2m	R	7	267-463	2.7
	350.55347-350.56666	PAIRITEL	J,H,Ks	3	300	2.6
04 , 12	351.61066-351.62334	1.2m	R	1	392	
04 , 13	352.74011-352.75118	1.2m	”	3	300	2.3
04 , 14	353.62542-353.63682	1.2m	”	”	”	2.0
04 , 15	354.68723-354.69858	1.2m	”	”	”	3.0
04 , 16	355.59923-355.61018	1.2m	”	”	”	2.5
04 , 18	358.32018-358.32590	INT	R	”	”	2.8
04 , 28	367.68095-367.69778	UKIRT	J,H,K	3	120	
04 , 30	370.32417-370.34623	WHT	R,I	1	270,270,540	2.0
05 Jan 7	378.45825-378.46899	TNG	R,I	7,3	180	1.4,1.2,1.1
05 , 14	384.57788-384.59612	MMT	r'	6,2	100	1.2,1.3
				3	300	1.0
QUIESCEENCE						
05 , 24	394.68693-394.71399	UKIRT	K	1	1620	0.7
05 Oct 25	669.32713-669.51805	WHT	R	5,20	300,600	1.4,1.2
05 Nov 24	698.90954-699.19509	Chandra	0.3-10 keV	1	24672	N/A

TABLE 2
EMISSION LINE PARAMETERS FROM THE AVERAGE SPECTRUM

Emission lines	γ (km s $^{-1}$)	(V _b +V _r)/2 (km s $^{-1}$)	V _r -V _b (km s $^{-1}$)	FWHM (Å)	FWZI (Å)	EW (Å)
H α	-122 ± 9	-53 ± 18	650 ± 40	30.4 ± 0.3	52 ± 3	6.5 ± 0.4
H β	-156 ± 18	-113 ± 49	370 ± 62	22 ± 1	35 ± 3	8 ± 2
HeII $\lambda 4686$	-67 ± 13^a	—	—	26 ± 1	33 ± 3	2.9 ± 0.2
H γ	-53 ± 35	—	—	24 ± 2	36 ± 3	1.5 ± 0.2
H δ	-142 ± 22	-193 ± 15	1075 ± 7	24 ± 1	31 ± 3	1.5 ± 0.4

^aAfter masking the emission spike on top of the line profile.

Note. — γ designates the positions (shifts) respect to the rest wavelength of the line and was measured with a Gaussian fit as the FWHM. V_b and V_r designate the shifts respect to the rest wavelength of the line of the blue and red peaks respectively and were measured using the task *splot* in IRAF.

TABLE 3
BEST-FITTING PARAMETERS OF THE QUIESCENT SPECTRUM OF J00291.

Model	Temp./PL index BB(keV), NSA (log K)	Unabsorbed 0.5-10 keV fluxes (10 $^{-14}$ ergs cm $^{-2}$ s $^{-1}$)	χ^2_{red} (d.o.f)	n.h.p (per cent)
BB	0.6 ± 0.2	3.8	3.4 (11)	0.01
NSA	$6.5^{+0.4}_{-0.2}$	3.9	3.2 (11)	0.02
PL	$2.4^{+0.5}_{-0.4}$	7.0	1.2 (11)	28

Note. — NSA, BB and PL stand for the neutron star atmosphere, blackbody and power-law models. Quoted uncertainties for the parameters of interest in these single component models are given at the 90 per cent confidence level ($\Delta\chi^2 = 2.71$). d.o.f. stands for degrees of freedom and n.h.p. for null hypothesis probability.